

Hydrogen desorption kinetics from monohydride and dihydride species on silicon surfaces

P. Gupta, V. L. Colvin, and S. M. George

Department of Chemistry, Stanford University, Stanford, California 94305

(Received 1 October 1987; revised manuscript received 21 December 1987)

Hydrogen desorption kinetics from monohydride and dihydride species on crystalline-silicon surfaces were measured using transmission Fourier-transform infrared (FTIR) spectroscopy. The FTIR desorption measurements were performed *in situ* in an ultrahigh-vacuum chamber using high-surface-area porous-silicon samples. The kinetics for hydrogen desorption from the monohydride and dihydride species was monitored using the SiH stretch mode at 2102 cm^{-1} and the SiH₂ scissors mode at 910 cm^{-1} , respectively. Annealing studies revealed that hydrogen from the SiH₂ species desorbed between 640 and 700 K, whereas hydrogen from the SiH species desorbed between 720 and 800 K. Isothermal studies revealed second-order hydrogen desorption kinetics for both the monohydride and dihydride surface species. Desorption activation barriers of 65 kcal/mol (2.82 eV) and 43 kcal/mol (1.86 eV) were measured for the monohydride and dihydride species, respectively. These desorption activation barriers yield upper limits of 84.6 kcal/mol (3.67 eV) and 73.6 kcal/mol (3.19 eV) for the Si—H chemical bond energies of the SiH and SiH₂ surface species.

I. INTRODUCTION

Hydrogen chemisorbed on silicon surfaces is of great fundamental and technological interest. In particular, hydrogen is known to passivate silicon surfaces by binding to silicon dangling bonds. This property is especially important in amorphous silicon where hydrogen reduces the density of defect states in the band gap.^{1,2}

The reduction of dangling bonds by hydrogen chemisorption may also dramatically affect silicon surface reactivity. For example, adsorbates such as NH₃,^{3,4} H₂O,^{5,6} PH₃,⁷ and C₃H₆ (Ref. 8) chemisorb dissociatively and form silicon-hydrogen bonds. The kinetics of these reactions are thought to be self-limiting as the product hydrogen atoms tie up silicon dangling bonds. Consequently, these reactions may be rate-limited by hydrogen desorption.

At higher hydrogen surface coverages, the SiH₂ species is encountered. This species is often associated with silicon surface reconstruction.⁹ Moreover, SiH₂ is believed to be a precursor in the etching of silicon surfaces.¹⁰ Thus an understanding of the relative stability and desorption kinetics of the monohydride and dihydride species on silicon surfaces is extremely important.

Previous ultraviolet photoemission-spectroscopy (UPS) and low-energy electron diffraction (LEED) studies⁹ have revealed different hydrogen phases on silicon surfaces as a function of hydrogen coverage. For example, on the Si(100) 2×1 surface, UPS studies have observed a monohydride phase where one hydrogen atom binds to each available silicon dangling bond. With continued exposure, the LEED pattern changes to a 1×1 structure suggesting that the Si—Si lateral surface bonds creating the 2×1 reconstruction have broken and dihydride species have formed. Electron-energy-loss spectroscopy (EELS) studies confirm the presence of dihydride species on both Si(111) 7×7 (Ref. 11) and Si(100) 2×1 .¹² Infrared studies on Si(100) 2×1 suggest that equal amounts

of hydrogen atoms exist in the monohydride and dihydride configurations at saturation hydrogen coverage.¹³

Previous temperature-programmed desorption (TPD) mass-spectrometric studies have measured an activation barrier of 59 kcal/mol (2.54 eV) for the desorption of H₂ from Si(111) 7×7 .¹⁴ Likewise, activation energies for the desorption of hydrogen from amorphous silicon have been measured by thermomanometric analysis,¹⁵ infrared spectroscopy,¹⁶ and mass spectrometry.¹⁷ Because hydrogen can exist in a variety of states in amorphous silicon,^{18–20} contradictory results have been obtained.

Mass-spectrometric studies cannot determine whether H₂ is desorbing from monohydride or dihydride species. In contrast, Fourier-transform infrared (FTIR) is sensitive to molecular structure and can distinguish between the monohydride and dihydride features. FTIR spectroscopy also has a typical frequency resolution of 4 cm^{-1} which is far better than the $40\text{--}60\text{ cm}^{-1}$ resolution limit for EELS. However, sensitivity requirements limit transmission FTIR spectroscopic studies to high-surface-area materials. Given typical infrared cross sections of $1\times 10^{-18}\text{ cm}^2$,²¹ single-crystal samples with approximately 1×10^{15} surface-atoms/cm² do not have a sufficient surface area for facile transmission infrared studies.

In order to obtain high-surface-area crystalline-silicon samples, porous silicon can be utilized. Porous silicon was first obtained by Uhler²² and Turner²³ by anodizing single-crystal silicon in dilute hydrofluoric acid. Transmission electron microscopy (TEM) micrographs have shown that porous silicon contains a network of nearly parallel pores approximately 200 Å in diameter with a center-to-center separation of approximately 300–400 Å.²⁴ Likewise, Brunauer-Emmett-Teller (BET) model methods have measured extremely high surface areas of approximately 205 m²/cm³ for porous silicon.²⁵ Other material properties of porous silicon have been characterized extensively and reported recently.^{26,27}

Under ordinary preparation conditions, porous silicon retains the crystallinity of the original silicon wafer.²⁸⁻³⁰ Furthermore, porous silicon exhibits sharp and pronounced infrared-absorption features that can be assigned unambiguously to silicon monohydride and dihydride surface species. In addition, the close correspondence between the infrared spectra of hydrogen on porous silicon and hydrogen on Si(100) 2×1 (Refs. 13 and 31-33) suggests that the surfaces of the porous silicon are very similar to Si(100) 2×1 .

In this work, transmission FTIR was used to monitor directly the temperature-dependent changes in the coverages of both monohydride and dihydride surface species on porous silicon. Concurrently, TPD mass-spectrometric studies observed the loss of surface hydrogen as H_2 in the gas phase. These FTIR studies enabled the desorption kinetics of H_2 from monohydride (SiH) and dihydride (SiH₂) species to be measured quantitatively.

II. EXPERIMENT

A. Preparation of porous silicon

The single-crystal silicon samples used to prepare porous silicon were (100) *p*-type boron-doped wafers produced by the Czochralski method. These Si(100) wafers had a resistivity of 0.464 Ω cm, a thickness of 380 μ m, and dimensions of 10×11 mm². A 2000-Å-thick film of tantalum was deposited on the back of the wafer by electron-beam evaporation. This thin tantalum film ensured a uniform current distribution during the electrochemical anodization. After completion of the anodization, part of this tantalum film was etched away from a circular area with a diameter of 7 mm at the center of the wafer to allow infrared transmission. In addition, two narrow strips (1.5×10 mm²) of tantalum were deposited along the front edges of the wafer. This ensured a good Ohmic contact for the subsequent resistive heating.

In order to prepare the porous silicon, the silicon wafer was placed in the Teflon sample holder as shown in Fig. 1. The sample holder was then immersed in a hydrofluoric acid solution for the anodic reaction. A

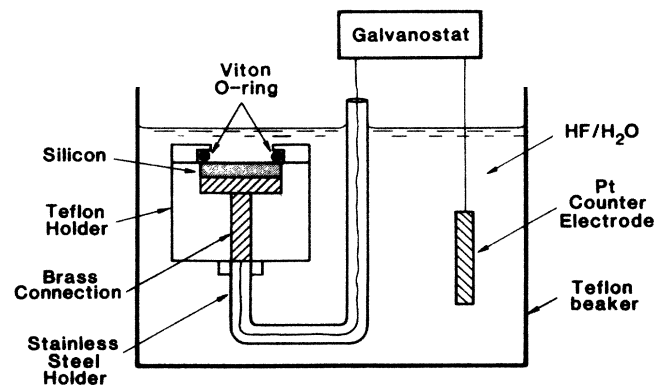


FIG. 1. Diagram of the experimental apparatus used to prepare porous-silicon samples. A porous layer with a 2 μ m thickness was produced with a current density of 200 mA/cm² for 15 s.

small circular opening in the sample holder with a diameter of 7 mm ensured that only a well-defined area on the silicon wafer was anodized. An O-ring seal between the wafer and the sample holder prevented leakage to other parts of the wafer.

An ultrasonic oscillator facilitated the removal of hydrogen bubbles from the surface of the porous-silicon samples. The electrolyte consisted of a 33% hydrofluoric-acid-ethanol mixture. A galvanostat provided a constant current of 200 mA/cm² and the anodization reaction was performed for 15 s. This current flux and time corresponded to a total charge flow of 1.12 C/cm².

The porous samples produced using the above conditions were bluish-grey in color in agreement with previous studies.²⁹ The thickness of the porous layer was 2 μ m as measured by cross-section scanning electron microscopy. This layer was extremely uniform and produced infrared interference fringes easily observed in the FTIR spectra.

B. UHV chamber for transmission FTIR

Prior to mounting the sample in the UHV chamber designed for transmission FTIR studies, the sample was rinsed successively in methanol, acetone, trichloroethylene, and hydrofluoric acid. The hydrofluoric acid was used to remove any native oxide which may have formed on the surface of the porous-silicon samples after anodization. The porous silicon was then mounted at the bottom of a liquid-nitrogen-cooled cryostat.

The edges of the porous-silicon sample were sandwiched on both sides between two strips of 0.001-in. tantalum foil. The tantalum foil, in turn, was clamped to a copper block. A molybdenum clip in the shape of a hair pin was fashioned using 0.010-in. molybdenum foil. This clip held the tantalum foil securely and uniformly to the edge of the porous-silicon sample.

The sample could be cooled to 100 K and heated to 1200 K using resistive heating. Temperatures were measured using a 0.005-in.-diam W-5% Re/W-26% Re thermocouple that was heliarc-welded onto the top edge of the silicon wafer. The temperature was maintained by a temperature controller that determined the voltage output of a HP 6264B programmable power supply (20 V, 20 A). The temperature controller could maintain temperatures to within ± 0.5 K or produce linear temperature ramps.

A schematic of the UHV chamber is shown in Fig. 2. The UHV chamber was pumped by a 190 l/s Balzers turbomolecular pump that was backed by another Balzers 50 l/s turbomolecular pump. This tandem turbomolecular pump system enabled pressures of 1.0×10^{-7} Torr to be obtained within 2 h after breaking vacuum. This facilitated a rapid turnaround time when changing samples.

The infrared beam passed through a pair of 0.5-in.-thick ZnSe windows. The ZnSe windows could be isolated from the vacuum chamber using gate valves. The use of gate valves was necessary to prevent species from being deposited inadvertently on the ZnSe windows. This was a problem during earlier oxidation studies when SiO desorbed from the porous-silicon samples at high temper-

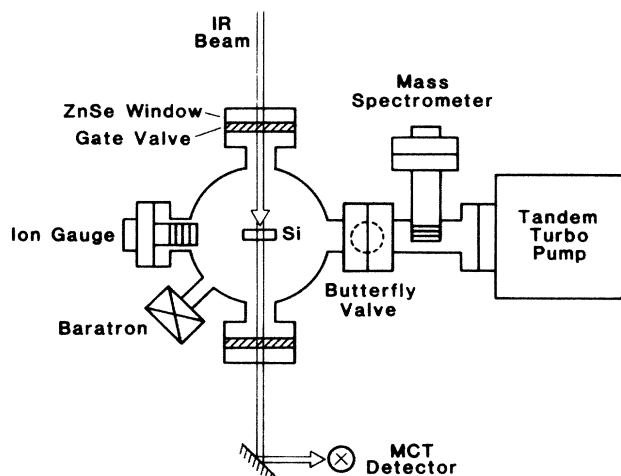


FIG. 2. Diagram of the UHV chamber for *in situ* transmission FTIR studies.

atures. Gas species such as SiO stick on the ZnSe windows and contribute spuriously to the FTIR spectra.

The UHV chamber was also equipped with a Dycor quadrupole mass spectrometer. The mass spectrometer was used to correlate the desorption of H₂ from the porous-silicon sample with changes in the silicon-hydrogen absorption features. An ion gauge was used to monitor the pressure of the chamber. The chamber was also equipped with a Baratron which enabled higher pressures of 10×10^{-2} Torr to be monitored. The reaction chamber could be isolated from the mass spectrometer and the tandem turbomolecular pumps by closing a butterfly valve.

The FTIR spectrometer employed in these studies was a Nicolet 7199. The relative advantages of using Fourier-transform infrared spectrometers over dispersive infrared instruments have been described elsewhere.³⁴ A high-sensitivity liquid-nitrogen-cooled mercury cadmium telluride (MCT) detector was employed. A total of 1024 scans were taken for each FTIR spectrum. The use of a MCT detector enabled high mirror velocities of 0.98 cm/s to be used which minimized the data-acquisition times.

Operating pressures for this FTIR work were typically 2.0×10^{-8} Torr. These pressures were reached in approximately 5 h after changing samples without baking the UHV chamber. These low pressures were critical for consistent results because porous-silicon samples can easily be oxidized at temperatures and pressures of oxygen as low as 200 K and 1×10^{-5} Torr, respectively.³⁵

C. Thermal annealing and isothermal annealing experiments

For the thermal annealing studies, the porous-silicon samples were raised to the annealing temperature, held at the annealing temperature for approximately 1 s and then returned to the initial temperature. The initial temperature of the porous-silicon sample was 300 K and a constant heating rate of 8 K/s was used to heat the sample. After returning to the initial temperature, a FTIR spectrum was taken. This experimental sequence was performed repeatedly for annealing temperatures up to 840

K.

Isothermal annealing experiments were carried out at various temperatures for both the monohydride and dihydride species. For the dihydride species, the temperatures ranged from 540 to 610 K. For the monohydride species, temperatures ranged from 690 to 730 K. In these experiments, the porous sample was raised to the isothermal temperature, held at that temperature for a given time, and then returned to the initial temperature of 300 K. A FTIR spectrum of the porous-silicon sample was then recorded to determine the coverage of the remaining silicon monohydride or silicon dihydride species. Using this procedure, the time-dependent coverage of the dihydride or monohydride species could be obtained as a function of temperature.

For the silicon monohydride isothermal annealing experiments, the sample was first heated to 640 K for 10 min. The integrated area under the 910-cm^{-1} SiH₂ scissors mode after such an isothermal anneal was zero. Thus this procedure removed the dihydride species and defined the initial coverage of the monohydride species. The subsequent integrated absorbances for the monohydride species were normalized using this initial monohydride coverage.

A new porous-silicon sample prepared under identical conditions was used for each annealing run. The total concentrations of monohydride and dihydride species on the surface were the same within 5% for each porous-silicon sample. These concentrations were determined using the integrated areas under the absorption peaks at 2110 and 910 cm^{-1} , respectively.

III. RESULTS

A. Infrared spectrum of porous silicon

After anodization, the porous-silicon samples exhibited pronounced infrared absorption features at 2087–2110 (doublet), 1107, 910, 666, and 625 cm^{-1} . Figure 3 shows a typical FTIR spectrum of a porous-silicon sample with

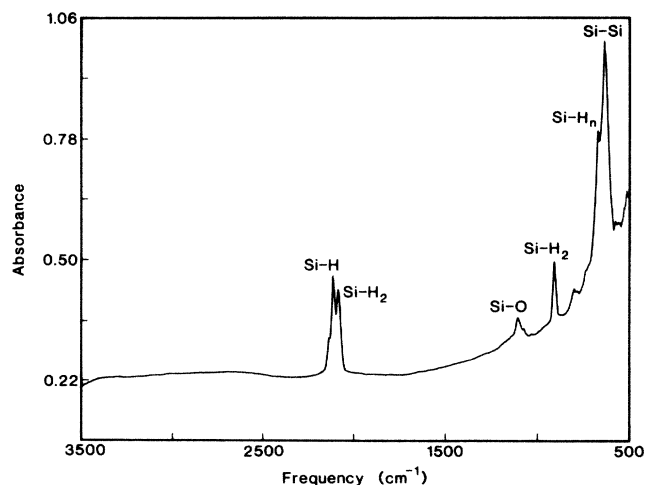


FIG. 3. Infrared spectrum of a porous-silicon sample. In order to enhance the infrared absorption features, a sample with a 6- μm -thick porous layer was utilized. This sample gave an absorbance approximately 3 times larger than usual.

a 6- μm -thick porous layer. For clarity of presentation, the absorbance of this sample was approximately three times larger than usual. Absorbance is defined as $A = -\log_{10}(I/I_0)$.

Early studies ascribed the 2087–2110 cm^{-1} doublet to silicon-hydrogen stretches.³⁶ Reflectance infrared studies of hydrogen on Si(100) 2×1 confirmed this suggestion.^{13,31–33,37} However, there has been some debate in the amorphous-silicon literature about the exact assignment of the absorption features around 2100 cm^{-1} .^{19,20,38,39} The thermal annealing studies discussed in the following section will show that the high-frequency component of the doublet originally at 2110 cm^{-1} can be assigned primarily to the silicon monohydride stretch. In addition, the correlation between the 2087 cm^{-1} and 910 cm^{-1} absorption features in the annealing studies will demonstrate that the low-frequency component of the doublet at 2087 cm^{-1} can be assigned primarily to the silicon dihydride stretch.

EELS studies on single-crystal silicon surfaces^{11,12} and infrared studies of gaseous silanes^{40,41} and amorphous silicon¹⁹ have observed the 910 cm^{-1} absorption feature. This absorption feature has been attributed to the scissors mode of the SiH_2 dihydride species. Likewise, EELS studies on Si(100) 2×1 (Ref. 12) and infrared studies on amorphous silicon¹⁹ and on porous silicon⁴² have assigned the absorptions at 666 and 625 cm^{-1} to the SiH or SiH_2 deformation modes.

A prominent Si-Si stretch mode was observed at 616 cm^{-1} in agreement with previous transmission infrared studies of single-crystal silicon.⁴³ Due to their close proximity, the two peaks at 625 and 616 cm^{-1} could not be resolved separately. However, after the thermal desorption of hydrogen from the monohydride and dihydride species, the absorption feature at 666 cm^{-1} was absent and the integrated area of the absorption feature at 616 cm^{-1} was reduced by a factor of 2.

The absorption at 1107 cm^{-1} has been attributed to a bulk interstitial Si-O-Si asymmetric stretch mode.^{44,45} This feature also appeared with equal intensity in unanodized silicon wafers following an HF etch. Consequently, this Si-O-Si feature is in the bulk of the silicon substrate and is not caused by oxygen on the porous-silicon surfaces.

A small shoulder appeared at 2140 cm^{-1} in the silicon-hydrogen stretching region. Although there was no evidence for a Si-O-Si surface species, this silicon-hydrogen stretch may be caused by the substituent effect of oxygen atoms. Similar blue shifts have been reported by infrared studies of amorphous silicon^{46,47} and by EELS studies of hydrogen on Si(100) 2×1 surfaces which had been previously exposed to oxygen.⁴⁸ However, annealing studies revealed that the desorption kinetics for this species and the dihydride species were similar. This suggests that the small shoulder may arise from another silicon dihydride stretching mode.

B. Thermal annealing

Figure 4 displays the changes in the FTIR spectra of porous silicon as a function of annealing temperature.

The FTIR spectra showed that the silicon dihydride species at 910 cm^{-1} have been removed from the surface by 720 K. On the other hand, the silicon monohydride species originally at 2110 cm^{-1} remained on the silicon surface until 820 K.

As the dihydride species is removed from the surface, the silicon monohydride stretch at 2110 cm^{-1} progressively shifted to 2102 cm^{-1} . There was no subsequent shift of this monohydride feature at 2102 cm^{-1} during the annealing and removal of the monohydride species. In addition, notice that the silicon-hydrogen stretching mode at 2087 cm^{-1} disappeared at nearly the same temperature as the scissors mode of the dihydride species at 910 cm^{-1} .

The thermal annealing data clearly demonstrated that the silicon monohydride and dihydride species were removed from the silicon surface at markedly different temperatures. When the silicon dihydride species began to decrease, a small increase was observed in the absorbance corresponding primarily to the silicon monohydride stretching mode. Given the second-order desorption kinetics measured for the dihydride species in Sec. III C, this increase is consistent with the conversion of two dihydride species to two monohydride species plus desorbed H_2 .

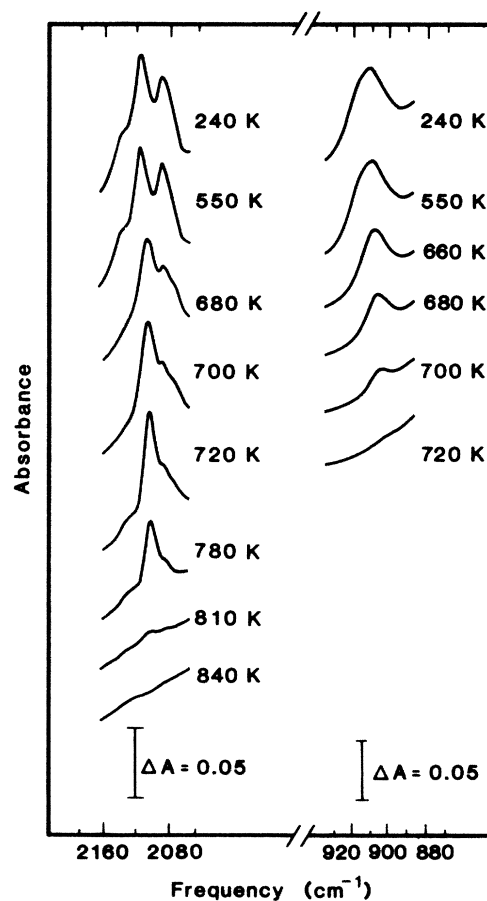


FIG. 4. Absorption spectra of porous silicon in the frequency ranges corresponding to the silicon-hydrogen stretching modes and silicon dihydride scissors mode as a function of annealing temperature.

A complete conversion of dihydride species to monohydride species should give a larger increase in the absorbance originally at 2110 cm^{-1} than the increase observed. However, as discussed in Sec. IV A, the spectral features in the silicon-hydrogen stretching region are congested when both species are present. Some monohydride and dihydride spectral features may be overlapping in the absorbance region around 2110 cm^{-1} . Consequently, monohydride kinetic studies were performed only after removing the dihydride species.

C. Isothermal annealing

Figure 5 shows the normalized integrated absorbance of the 910 cm^{-1} scissors mode for the SiH_2 species as a function of time for five different temperatures. The decrease of the integrated absorbance of the 910-cm^{-1} mode reflects the isothermal desorption of H_2 from the dihydride species. Second-order rate equations of the form $-d\Theta/dt = k\Theta^2$ were used to fit the data points.

For convenience, the initial coverages Θ_0 (cm^{-2}) were normalized to $\Theta'_0 = 1$. Consequently, integrated second-order fits of the form $\Theta'(t) = 1/(1+k't)$ were utilized. The rate constants k' obtained using this normalized form can be converted to absolute rate constants k by $k = k'/\Theta_0$.

The second-order fits to the data are shown as solid lines in Fig. 5. The fits are very good and clearly reveal that hydrogen desorption from the dihydride species occurs with second-order kinetics. In contrast, earlier studies reported first-order kinetics for hydrogen desorption from the dihydride species.^{14,16}

Each curve in Fig. 5 corresponds to the isothermal desorption of hydrogen from the silicon dihydride species at one particular temperature. These curves reflect the various temperature-dependent rate constants for hydrogen desorption. The Arrhenius plot of the rate constants

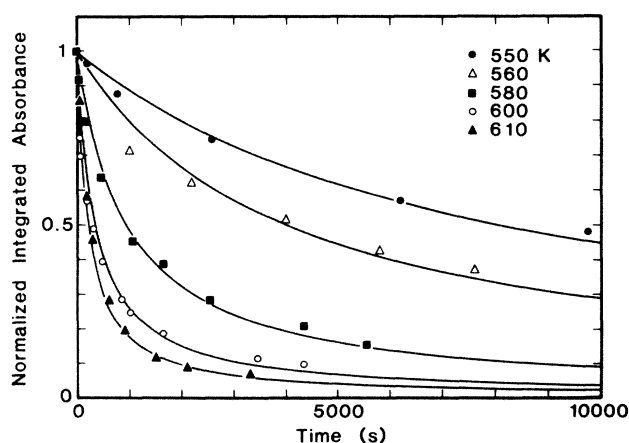


FIG. 5. Isothermal desorption of hydrogen from the silicon dihydride species measured by monitoring the normalized integrated absorbance of the silicon dihydride scissors mode at 910 cm^{-1} as a function of time at different temperatures. The solid lines show the fit of a second-order rate law of the form $-d\Theta/dt = k\Theta^2$ to the data. A normalized integrated rate law given by $\Theta'(t) = 1/(1+k't)$ where $k' = k\Theta_0$ was utilized.

is displayed in Fig. 6(a).

Within the temperature range of this experiment, Fig. 6(a) shows that hydrogen desorption follows Arrhenius behavior given by $k = \nu_2 \exp(-E_{\text{des}}/RT)$. The activation barrier for hydrogen desorption from the silicon dihydride species was $E_{\text{des}} = 43\text{ kcal/mol}$ (1.86 eV). Assuming an initial dihydride coverage of $\Theta_0 = 2.3 \times 10^{14}\text{ cm}^{-2}$, the preexponential for hydrogen desorption from the silicon dihydride species was $4.7 \times 10^{-2}\text{ cm}^2/\text{s}$. The choice of this initial dihydride coverage is justified in Sec. III D.

Figure 7 shows the normalized integrated absorbance of the silicon monohydride stretch at 2102 cm^{-1} as a function of time for five different temperatures. The decrease of the integrated absorbance of this mode reflects isothermal desorption of hydrogen from silicon monohydride species. Like the isothermal data for the dihydride species, a second-order rate equation fits the data points very accurately. These fits are shown as solid lines in Fig. 7.

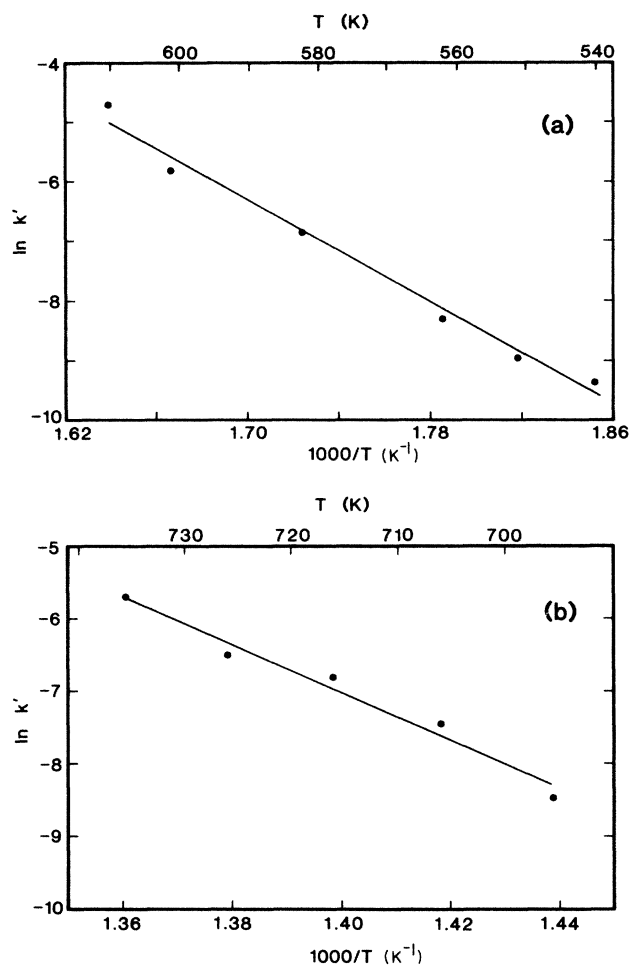


FIG. 6. Arrhenius plot of the temperature-dependent rate constants k' for hydrogen desorption from (a) dihydride species and (b) monohydride species. The measured activation barrier for desorption from the silicon dihydride species was $E_{\text{des}} = 43\text{ kcal/mol}$ (1.86 eV). The measured activation barrier for desorption from the silicon monohydride species was $E_{\text{des}} = 65\text{ kcal/mol}$ (2.82 eV).

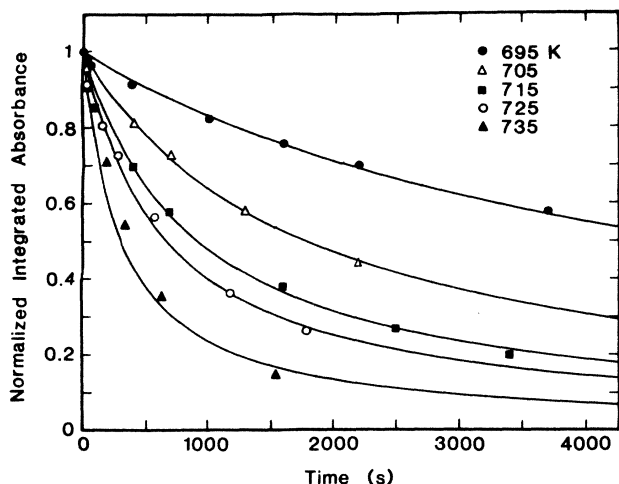


FIG. 7. Isothermal desorption of hydrogen from silicon monohydride species measured by monitoring the normalized integrated absorbance of the silicon monohydride stretch at 2102 cm^{-1} as a function of time at different temperatures. The solid lines display the fit of a second-order rate law of the form $-d\Theta/dt = k\Theta^2$. A normalized integrated rate law given by $\Theta'(t) = 1/(1+k't)$ where $k' = k\Theta_0$ was employed.

Figure 6(b) shows the Arrhenius plot of the temperature-dependent rate constants for the isothermal desorption of hydrogen from the monohydride species. The activation barrier for hydrogen desorption from the monohydride species was $E_{\text{des}} = 65\text{ kcal/mol}$ (2.82 eV). Assuming an initial monohydride coverage of $\Theta_0 = 6.8 \times 10^{14}\text{ cm}^{-2}$, the preexponential for hydrogen desorption from the monohydride species was $1.7 \times 10^2\text{ cm}^2/\text{s}$. This initial monohydride coverage is equivalent to the number of silicon atoms in the uppermost layer on a $\text{Si}(100)$ surface.

Figure 8 shows the correlation between the low-frequency component of the doublet in the silicon-hydrogen stretching region at 2087 cm^{-1} and the dihydride scissors mode at 910 cm^{-1} . The normalized integrated absorbances of the absorption features at 2087 and 910 cm^{-1} are plotted as a function of temperature and time, respectively, in Figs. 8(a) and 8(b). The integrated absorbance of the 2087-cm^{-1} peak was obtained by subtracting the integrated absorbance of the monohydride species from the total integrated absorbance. When the integrated absorbance of the dihydride scissors mode at 910 cm^{-1} was zero, the monohydride contribution was defined as the integrated absorbance of the remaining 2102-cm^{-1} peak.

D. Mass-spectrometry studies

Mass-spectrometric analysis demonstrated that the desorption of H_2 correlates well with the disappearance of the silicon-hydrogen infrared bands. Figure 9 displays the correlation between the mass-spectrometric measurement of the integrated desorption of H_2 evolving from the monohydride species and the disappearance of the integrated absorbance for the monohydride stretch. Figure

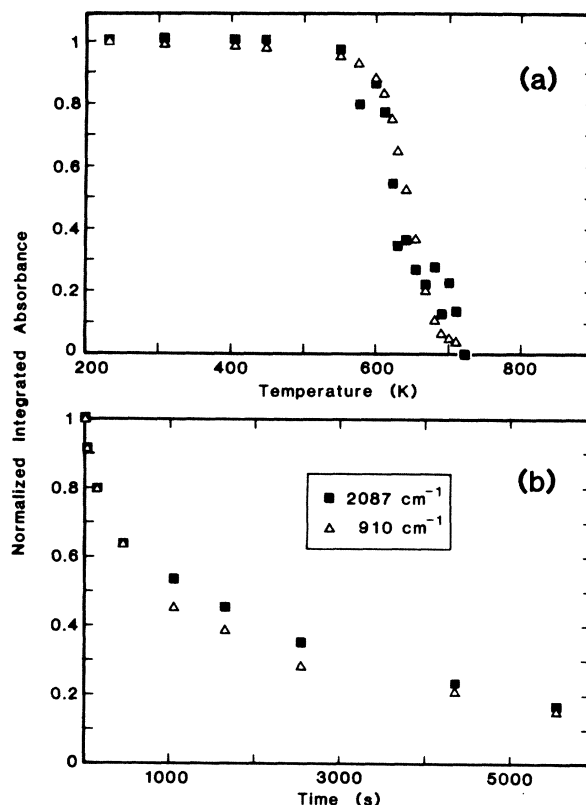


FIG. 8. Normalized integrated absorbance of the absorption at 2087 cm^{-1} in the silicon-hydrogen stretching region and the absorption at 910 cm^{-1} assigned to the silicon dihydride scissors mode as (a) a function of annealing temperatures and (b) a function of time at 580 K .

9 confirms that the infrared cross sections for the silicon-hydrogen stretch remain constant as a function of surface hydrogen coverage.

The combined infrared and mass-spectrometric analysis also revealed that there is a 3:1 ratio between H_2 desorbing from monohydride and dihydride species. The

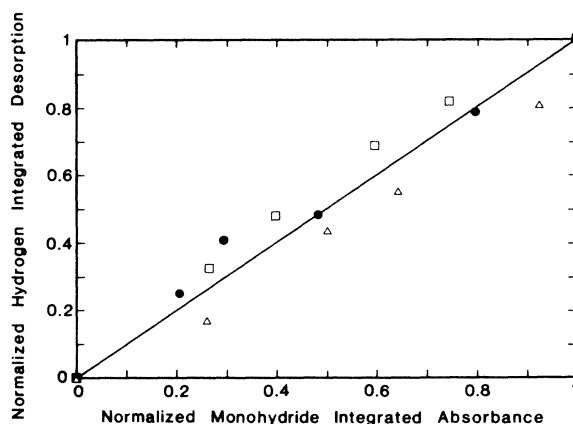


FIG. 9. Correlation between the mass-spectrometric measurement of hydrogen integrated desorption and the infrared measurement of hydrogen disappearance from the surface. The data are from three porous-silicon samples using the integrated absorbance of the silicon monohydride stretch.

desorption kinetics is second-order for H_2 desorption from both monohydride and dihydride species. Following the recombinatory desorption of H_2 from two dihydride species, the two dihydride species would be converted to two monohydride species. Consequently, given a 3:1 ratio for H_2 desorbing from monohydride and dihydride species, the initial ratio between the number densities for the monohydride and dihydride surface species on porous silicon is 2:1.

An initial ratio of 2:1 between monohydride (SiH) and dihydride (SiH₂) species indicates that equal amounts of hydrogen atoms reside in each species. Previous infrared studies of hydrogen on Si(100) at saturation hydrogen coverage have measured a 1:1 ratio between monohydride and dihydride configurations.¹³ On Si(100), silicon surface atoms dimerize and form the 2×1 reconstruction. The resulting monohydride configuration on Si(100) consists of a silicon dimer (H-Si-Si-H) with one hydrogen per silicon.⁹ In agreement with the above results, these previous infrared measurements indicate that equal amounts of hydrogen atoms exist in each configuration.

IV. DISCUSSION

A. Infrared spectra of porous silicon

A comparison of the infrared spectra of hydrogen chemisorbed on Si(111) 7×7 , Si(100) 2×1 , and porous silicon reveals that hydrogen chemisorbed on Si(100) 2×1 and porous silicon are remarkably similar.^{13,31-33} The infrared spectra of hydrogen on Si(100) 2×1 and on porous silicon both display a sharp and distinct doublet structure in the silicon-hydrogen stretching region at nearly the same frequencies. Moreover, the sharp structure suggests well-defined hydrogen chemisorption sites.

In contrast, the infrared spectra of hydrogen on Si(111) 7×7 is characterized by a rather broad, featureless, absorption centered around 2100 cm^{-1} .⁴⁹ This broad distribution indicates that hydrogen is chemisorbed in an inhomogeneous distribution of sites. Consequently, the similarity in structure and close correspondence in frequencies suggest that the surface of porous silicon is similar to Si(100) 2×1 .

A simple thermodynamic explanation argues that the hydrogenated Si(100) surface would be favored in porous-silicon formation. For example, the unreconstructed Si(100) surface has a higher density of silicon dangling bonds than the other low-Miller-index silicon surfaces such as the unreconstructed Si(111) and Si(110) surfaces. Therefore, because Si—H bond energies are larger than bulk Si—Si bond energies,⁵⁰ the hydrogenated Si(100) surface is more stable than the hydrogenated Si(111) and Si(110) surfaces.

Infrared studies of hydrogenated Si(100) 2×1 surfaces have shown that, because of the dimer structure on the surface, the monohydride silicon-hydrogen stretch is characterized by two modes.³³ One mode is the antisymmetric stretch with a transition dipole moment parallel to the surface along the dimer direction. The other mode is the symmetric stretch with a transition dipole moment perpendicular to the surface. The antisymmetric and symmetric modes have transition frequencies at 2088 and

2099 cm^{-1} , respectively.³³ Cluster calculations have confirmed these assignments and the difference in frequencies.³³

The dihydride silicon-hydrogen stretch on Si(100) 2×1 is also characterized by two modes. One mode is the antisymmetric stretch with a transition dipole moment parallel to the surface. The other mode is the symmetric stretch with a transition dipole moment perpendicular to the surface. The antisymmetric and the symmetric dihydride stretching modes have their transition frequencies at 2104 and 2091 cm^{-1} , respectively.¹³

The thermal stability of the monohydride species is expected to be higher than the dihydride species. Consequently, the silicon-hydrogen stretch on porous silicon at 2102 cm^{-1} after the removal of the dihydride species is assigned to a monohydride species. Likewise, the correlation between the desorption kinetics for the absorption features at 2087 and 910 cm^{-1} argue that the silicon-hydrogen stretch on porous silicon at 2087 cm^{-1} is associated with a dihydride species.

The desorption behavior, the similarity of the spectral features, and the above frequency assignments suggest the following correspondence between porous silicon and Si(100) 2×1 . The monohydride absorption feature on porous silicon at 2102 cm^{-1} is closely associated with the symmetric monohydride feature on Si(100) 2×1 at 2099 cm^{-1} . Likewise, the dihydride absorption feature on porous silicon at 2087 cm^{-1} compares favorably with the symmetric dihydride feature on Si(100) 2×1 at 2091 cm^{-1} . Thus we believe that no antisymmetric modes are clearly observed in our FTIR spectra of hydrogen on porous silicon.

The selectivity for symmetric vibrational modes can be explained by considering the experimental geometry. The FTIR experiments were performed with the infrared light impinging on the silicon wafer at normal incidence. Because the pores are primarily normal to the surface of the silicon wafer, the passage of infrared light through the pores can be regarded as nearly equivalent to an external grazing incidence geometry.

Using expressions derived by Chabal,³² the change in the reflectance ΔR can be calculated for light polarized both parallel (ΔR_{\parallel}) and perpendicular (ΔR_{\perp}) to the plane of incidence for a given vibrational oscillator. A model calculation was performed assuming an isotropic Si-H vibrational oscillator with an angle of incidence of $\theta = 85^\circ$. At this angle close to grazing incidence, ΔR_{\perp} was found to be negligible compared to ΔR_{\parallel} .

The infrared light used in this FTIR study was not polarized. However, the model calculation demonstrates that the maximum changes in reflectivity at close to grazing incidence will be obtained for light that is polarized parallel to the plane of incidence (ΔR_{\parallel}). Light of this polarization interacts with vibrational modes which are perpendicular to the surface. Thus the external grazing incidence geometry discriminates in favor of the symmetric vibrational modes.

The integrated area under the silicon monohydride peak at 2102 cm^{-1} and the gas-phase cross section for a silicon-hydrogen stretch can be used to approximate the concentration of monohydride species on the porous sil-

icon after removing the dihydride species by thermal annealing. Using a gas-phase cross section of 6.35×10^{-19} cm² for the Si—H bond,^{19,21} typical monohydride concentrations of 1.81×10^{21} cm⁻³ were determined for the 2- μ m-thick porous layer.

The monohydride coverage after the thermal anneal of the dihydride species was assumed to correspond to the number of silicon atoms in the uppermost layer on Si(100) or a coverage of 6.8×10^{14} cm⁻². Consequently, a surface area of 268 m²/cm³ was calculated for the porous silicon. This surface area agrees well with the surface-area measurement of 205 m²/cm³ obtained using BET methods for porous silicon prepared under similar conditions.^{25,27}

B. Desorption kinetics

Second-order kinetics for hydrogen desorbing from silicon monohydride species are anticipated. Two hydrogen atoms from two adjacent silicon monohydride species must recombine in order to form H₂. Second-order kinetics for recombinatory desorption should be observed in the absence of adsorbate-adsorbate interactions or site inhomogeneities. Likewise, second-order desorption kinetics are commonly observed in the recombinatory desorption of hydrogen from transition-metal surfaces.^{51–53}

Second-order desorption kinetics from the silicon dihydride species is a new observation. Previous studies had suggested that the H₂ desorption from dihydride species was first-order in the silicon dihydride coverage.^{14,16} The rationalization for first-order kinetics was that the desorbing H₂ molecule was formed by the association of two hydrogen atoms from the same dihydride species.^{14,16} In contrast, theoretical work recently modeled the desorption of H₂ from dihydride species on Si(100) in terms of the recombinatory desorption of two hydrogen atoms from two adjacent silicon dihydride species.⁵⁴ This model predicts second-order desorption kinetics in agreement with the experimental observations.

The activation barrier of 65 kcal/mol (2.82 eV) measured for H₂ desorption from monohydride species is in reasonably good agreement with previously measured activation barriers. For example, an activation barrier of 59 kcal/mol (2.54 eV) for H₂ desorption from Si(111) 7 \times 7 was determined using temperature programmed desorption.¹⁴ An activation barrier of 61 kcal/mol (2.60 eV) for H₂ desorption from Si(111) 7 \times 7 was recently measured by using laser-induced thermal desorption techniques.⁵⁵ Likewise, variational transition rate calculations have predicted an activation barrier of 55.6 kcal/mol (2.41 eV) for hydrogen desorbing from Si(111).⁵⁶

The chemical binding energy of a hydrogen molecule is 104.2 kcal/mol (4.52 eV). If the activation barrier of desorption, E_{des} is equal to the heat of adsorption, E_{ad} , the silicon-hydrogen chemical bond energy can be obtained using $2E(\text{Si—H}) = E_{\text{des}} + E(\text{H—H})$. The main assumption behind this determination of the Si—H chemical bond energy is the absence of an activation barrier for adsorption.

If an activation barrier for adsorption exists, then $E_{\text{des}} > E_{\text{ad}}$ and the silicon-hydrogen chemical ener-

gies will be overestimated. Consequently, upper limit values of 84.6 kcal/mol (3.67 eV) and 73.6 kcal/mol (3.19 eV) are obtained for the silicon-hydrogen bond energies of the SiH and SiH₂ surface species, respectively. A recent theoretical calculation has predicted an activation barrier of 4.2 kcal/mol (0.182 eV) for hydrogen adsorption on Si(111).⁵⁶ Using this activation barrier for adsorption, chemical bond energies of 82.5 kcal/mol (3.58 eV) and 71.5 kcal/mol (3.10 eV) are obtained for the silicon-hydrogen bond energies of the SiH and SiH₂ surface species.

These silicon-hydrogen chemical bond energies are well inside the 64–90 kcal/mol range obtained for SiH and SiH₂ bond strengths in gas-phase silanes.⁵⁰ This agreement suggests that silicon-hydrogen bond breaking does not occur as a concerted process with the reconstruction or dimerization of surface silicon atoms. If desorption and reconstruction or dimerization were concurrent, then the energy gained by the reconstruction or dimerization would lower the desorption activation barrier considerably. Consequently, an unreasonably low value for the silicon-hydrogen bond strength would be obtained.

Finally, the kinetic parameters for H₂ desorption from monohydride and dihydride species on porous-silicon surfaces were used to generate a TPD curve. Figure 10 shows the predicted hydrogen TPD signal for a heating rate of 6.6 K/s and a coverage equivalent to the initial hydrogen coverage on porous silicon. Dihydride and monohydride desorption parameters were used to generate the low-temperature (β_2) and the high-temperature (β_1) hydrogen desorption curves, respectively.

This simulated TPD curve is nearly identical to the measured TPD spectrum of hydrogen on Si(111) 7 \times 7 obtained at saturation hydrogen coverage with a heating rate of 6.6 K/s.^{14,55} Likewise, this simulation is also nearly equivalent to the TPD spectrum of hydrogen on Si(100) 2 \times 1 obtained at saturation coverage with a heat-

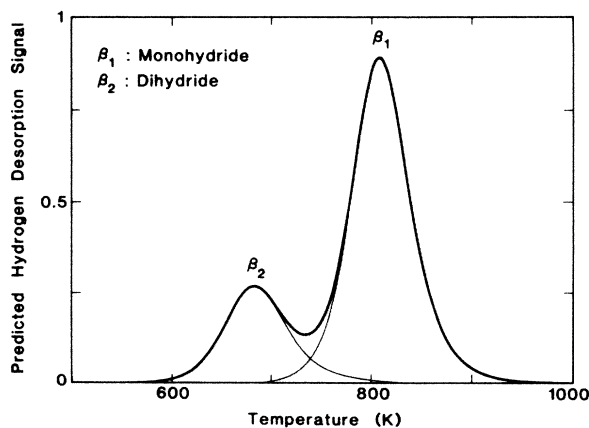


FIG. 10. Predicted hydrogen temperature programmed desorption (TPD) signal from a silicon surface using the dihydride and monohydride desorption kinetics obtained from this study. The initial coverages were defined to yield a 3:1 ratio for H₂ evolving from monohydride and dihydride species. A heating rate of 6.6 K/s was utilized.

ing rate of 12.5 K/s.⁵⁷ This agreement argues that the high-temperature β_1 peak commonly observed in TPD studies of hydrogen on single-crystal silicon surfaces is H₂ desorbing recombinatively from monohydride species. Likewise, the agreement suggests that the low-temperature β_2 peak observed in the TPD spectra is H₂ desorbing recombinatively from dihydride species.

V. CONCLUSIONS

The kinetics for hydrogen desorption from monohydride and dihydride species on crystalline-silicon surfaces were measured using transmission FTIR Spectroscopy. The desorption studies were performed *in situ* in an UHV chamber using high-surface-area porous-silicon samples. Hydrogen on the porous-silicon surface was observed to be very similar to hydrogen on Si(100) 2×1.

The kinetics for hydrogen desorption from the monohydride and dihydride species were monitored using the SiH stretch at 2102 cm⁻¹ and SiH₂ scissor mode at 910 cm⁻¹, respectively. Annealing studies revealed that the SiH₂ species desorbed between 640 and 700 K, whereas the SiH species desorbed from the silicon surface between 720 and 800 K. Isothermal studies revealed second-order desorption kinetics from both the monohydride and dihydride species.

A desorption activation barrier of 65 kcal/mol (2.82 eV) and a preexponential of 1.7×10² cm²/s were measured for H₂ desorbing from the monohydride species. A desorption activation barrier of 43 kcal/mol (1.86 eV) and a preexponential of 4.7×10⁻² cm²/s were measured for H₂ desorbing from the dihydride species. These desorption activation barriers yield upper limits of 84.6 kcal/mol (3.67 eV) and 73.6 kcal/mol (3.19 eV) for the silicon-hydrogen chemical bond energies of SiH and SiH₂ surface species.

ACKNOWLEDGMENTS

This work was supported in part by the Office of Naval Research under Contracts No. N00014-86-K-737 and No. N00014-86-K-545. Some of the equipment utilized in this work was provided by the National Science Foundation—Materials Research Laboratory Program through the Center for Materials Research at Stanford University. Partial funding for the construction of the UHV chamber for *in situ* transmission FTIR studies was provided by Exxon Research and Engineering Company. We thank Professor N. S. Lewis and his co-workers for providing the electrochemical instrumentation used to prepare porous silicon. We also acknowledge Dr. Y. J. Chabal for many useful discussions.

- ¹H. Fritzche, C. C. Tsai, and P. Pearson, *Solid State Technol.* **21**, 55 (1978).
- ²D. E. Carlson and C. R. Wronski, *J. Electron. Mater.* **6**, 2 (1977).
- ³L. Kubler, E. K. Hill, D. Bolmont, and G. Gewinner, *Surf. Sci.* **183**, 503 (1987).
- ⁴F. Bozso and Ph. Avouris, *Phys. Rev. Lett.* **57**, 1185 (1986).
- ⁵Y. J. Chabal and S. B. Christman, *Phys. Rev. B* **29**, 6974 (1984).
- ⁶H. Ibach, Wh. Wagner, and D. Bruchmann, *Solid State Commun.* **42**, 457 (1982).
- ⁷M. L. Yu and B. S. Meyerson, *J. Vac. Sci. Technol. A* **2**, 446 (1984).
- ⁸M. J. Bozack, W. J. Choyke, L. Muehlhoff, and J. T. Yates, Jr., *Surf. Sci.* **176**, 547 (1986).
- ⁹T. Sakurai and H. D. Hagstrum, *Phys. Rev. B* **14**, 1593 (1976).
- ¹⁰H. Kobayahi, K. Edamoto, M. Onchi, and M. Nishijima, *J. Chem. Phys.* **78**, 7429 (1983).
- ¹¹H. Wagner, R. Butz, U. Backes, and D. Bruchmann, *Solid State Commun.* **38**, 1155 (1981).
- ¹²F. Stucki, J. A. Schaefer, J. R. Anderson, G. J. Lapeyre, and W. Gopel, *Solid State Commun.* **47**, 795 (1983).
- ¹³Y. J. Chabal and K. Raghavachari, *Phys. Rev. Lett.* **54**, 1055 (1985).
- ¹⁴G. Schulze and M. Henzler, *Surf. Sci.* **124**, 336 (1983).
- ¹⁵J. A. McMillan and E. M. Peterson, *J. Appl. Phys.* **50**, 5238 (1979).
- ¹⁶D. Masson, L. Paquin, S. Poulin-Dandurand, E. Sacher, and A. Yelon, *J. Non-Cryst. Solids* **66**, 93 (1984).
- ¹⁷M. H. Brodsky, M. A. Frisch, W. A. Lanford, and J. F. Ziegler, *Appl. Phys. Lett.* **30**, 561 (1977).
- ¹⁸J. A. Reimer, R. W. Vaughan, and J. C. Knights, *Phys. Rev. B* **24**, 3360 (1984).
- ¹⁹M. H. Brodsky, M. Cardona, and J. J. Cuomo, *Phys. Rev. B* **16**, 3356 (1977).
- ²⁰H. Shanks, C. J. Fang, L. Ley, M. Cardona, F. J. Demond, and S. Kalbitzer, *Phys. Status Solidi* **100**, 43 (1980).
- ²¹L. A. Pugh and K. N. Rao, *Molecular Spectroscopy: Modern Research*, edited by K. N. Rao (Academic, New York, 1976), Vol. II.
- ²²A. Uhlir, *Bell Syst. Tech. J.* **35**, 333 (1956).
- ²³D. R. Turner, *J. Electrochem. Soc.* **105**, 402 (1958).
- ²⁴M. I. J. Beale, N. G. Chew, M. J. Uren, A. G. Cullis, and J. D. Benjamin, *Appl. Phys. Lett.* **46**, 86 (1985).
- ²⁵G. Bomchil, R. Herino, K. Barla, and J. C. Pfister, *J. Electrochem. Soc.* **130**, 1161 (1983).
- ²⁶K. Barla, R. Herino, G. Bomchil and J. C. Pfister, *J. Cryst. Growth* **68**, 727 (1984).
- ²⁷V. Labunov, V. Bondarenko, L. Glinenko, A. Dorofeev, and L. Jabulina, *Thin Solid Films* **137**, 123 (1986).
- ²⁸I. M. Young, M. I. J. Beale, and J. E. Benjamin, *Appl. Phys. Lett.* **46**, 1133 (1985).
- ²⁹R. W. Hardeman, M. I. J. Beale, D. B. Gasson, J. M. Keen, C. Pickering, and D. J. Robbins, *Surf. Sci.* **152**, 1051 (1985).
- ³⁰K. Barla, G. Bomchil, R. Herino, and J. C. Pfister, *J. Cryst. Growth* **68**, 721 (1984).
- ³¹Y. J. Chabal, *J. Vac. Sci. Technol. A* **3**, 1148 (1985).
- ³²Y. J. Chabal, in *Semiconductor Interfaces: Formation and Properties* (Springer-Verlag, New York, 1987).
- ³³Y. J. Chabal and K. Raghavachari, *Phys. Rev. Lett.* **53**, 282 (1984).
- ³⁴A. T. Bell, in *Vibrational Spectroscopy for Adsorbed Species*, Vol. 137 of *ACS Symposium Series*, edited by A. T. Bell and M. L. Hair (American Chemical Society, Washington, D.C., 1980).
- ³⁵P. Gupta, V. L. Colvin, and S. M. George (unpublished).
- ³⁶K. H. Beckmann, *Surf. Sci. Sci.* **3**, 314 (1965).

- ³⁷G. E. Becker and G. W. Gobeli, *J. Chem. Phys.* **38**, 2942 (1963).
- ³⁸S. Oguz, R. W. Collins, M. A. Paesler, and W. Paul, *J. Non-Cryst. Solid* **35**, 231 (1980).
- ³⁹W. Paul, *Solid State Commun.* **34**, 283 (1980).
- ⁴⁰E. A. V. Ebsworth, M. Onyszchuk, and N. Sheppard, *J. Chem. Soc.* **14**, 53 (1958).
- ⁴¹C. Tindal, J. Straley, and H. N. Nielsen, *Phys. Rev.* **62**, 151 (1942).
- ⁴²P. B. Harwood and G. P. Thomas, in *Materials Issues in Silicon Integrated Circuit Processing*, Vol. 71 of *Materials Research Society Symposium Proceedings*, edited by M. Wittmer, J. Stimmell, and M. Strathman (Materials Research Society, Pittsburgh, 1986).
- ⁴³R. J. Collins and H. Y. Fan, *Phys. Rev.* **93**, 674 (1954).
- ⁴⁴H. J. Hrostowski and R. H. Kaiser, *Phys. Rev.* **107**, 966 (1957).
- ⁴⁵W. Kaiser, P. H. Keck, and C. F. Lange, *Phys. Rev.* **101**, 1264 (1956).
- ⁴⁶G. Lucovsky, J. Yang, S. S. Chao, J. E. Tyler, and W. Czuba-tyj, *Phys. Rev. B* **28**, 3225 (1983).
- ⁴⁷P. John, I. M. Odeh, M. J. K. Thomas, M. J. Tricker, and J. I. B. Wilson, *Phys. Status Solidi* **105**, 499 (1981).
- ⁴⁸J. A. Schaefer, J. Frankel, F. Stucki, W. Gopel, and G. J. Lapeyre, *Surf. Sci.* **139**, L209 (1984).
- ⁴⁹Y. J. Chabal, G. S. Higashi, and S. B. Christman, *Phys. Rev. B* **28**, 4472 (1983).
- ⁵⁰R. Walsh, *Acc. Chem. Res.* **14**, 246 (1981).
- ⁵¹P. Feulner and D. Menzel, *Surf. Sci.* **154**, 465 (1985).
- ⁵²K. Christmann, O. Schober, G. Ertl, and M. Neumann, *J. Chem. Phys.* **60**, 4528 (1974).
- ⁵³K. Christmann, G. Ertl, and T. Pignet, *Surf. Sci.* **54**, 365 (1976).
- ⁵⁴S. Ciraci and I. Batra, *Surf. Sci.* **178**, 80 (1986).
- ⁵⁵B. G. Koehler, C. H. Mak, D. A. Arthur, P. A. Coon, and S. M. George, *J. Chem. Phys.* (to be published).
- ⁵⁶L. M. Raff, I. NoorBatcha, and D. L. Thompson, *J. Chem. Phys.* **85**, 3081 (1986).
- ⁵⁷J. Leifels, Dissertation, University of Hannover, Federal Republic of Germany, 1984.

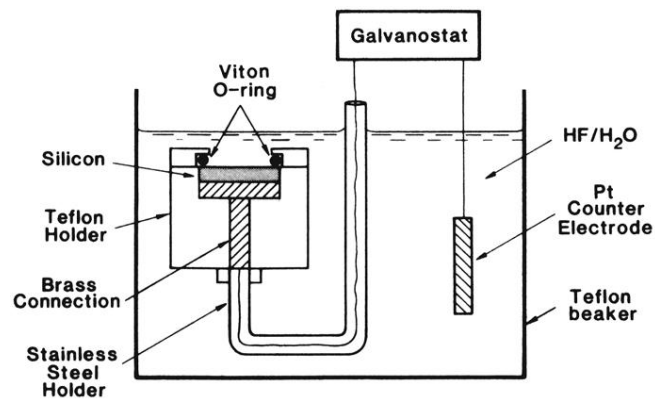


FIG. 1. Diagram of the experimental apparatus used to prepare porous-silicon samples. A porous layer with a $2\ \mu\text{m}$ thickness was produced with a current density of $200\ \text{mA}/\text{cm}^2$ for 15 s.